Imaging by Diffraction in Transmission Electron Microscopy

Jung Cho, Ambarneil Saha, Matthew Mecklenburg

Microscopy and Microanalysis, **30** (Suppl 1), 2024, 325–326
https://doi.org/10.1093/mam/ozae044.148

Microscopy AND Microanalysis

Meeting-report

Imaging by Diffraction in Transmission Electron Microscopy

Jung Cho[1], Ambarneil Saha[2], and Matthew Mecklenburg[1,*]

[1]*California NanoSystems Institute (CNSI), University of California, Los Angeles, CA, USA*
[2]*National Center for Electron Microscopy, Molecular Foundry, Lawrence Berkeley National Laboratory, Berkeley, CA, USA*
*Corresponding author: mmecklenburg@cnsi.ucla.edu

The purpose of crystallography is to produce an image [1]. The generation of an image requires a Fourier transform and an inverse Fourier transform with some optical phase distortions added to the latter transform that limit the final resolution. The phase-less diffraction data collected through conventional crystallographic means is the result of a real space Fourier transform. This data is processed through various methods to assign a phase to the peaks in reciprocal space [2]. This phase assignment, outside of the microscope, is what facilitates the production of the final image (a density or potential map) of the basis unit in the crystal. The transformations from real space to reciprocal space and back are analogous to the same processes in conventional transmission electron microscopy (TEM) and scanning transmission electron microscopy (STEM) where the sample and source are imaged, respectively.

When using the microscope optics to assign the limiting phase, we are bound by aberrations and coherence (typically 1 Angstrom or 10 1/nm in an uncorrected TEM). Aberration correction and monochromation can extend this by modifying the phase of the electron wave (0.4 Å or 25 1/nm). Using crystallographic direct methods [2], we are only limited by diffraction (about 0.2 Å or 50 1/nm). The limitation of diffraction scattering is a bit ambiguous because the crystal defects, thickness, temperature, and the objective electromagnet's bore diameter can all set this boundary. 4DSTEM, an addition of 2-dimensional raster imaging with STEM and 2-dimensional diffraction acquisitions at each point, blends these techniques.

Which method is best? Of course, this depends on the application. Real space imaging is the only choice for amorphous materials or when examining interfaces and defects. However, this modality requires exceedingly high electron fluxes of $\sim 10^8$ $e^-/Å^2/s$ (10 pA in a 1 Å diameter probe), and destruction of radiolysis sensitive materials will occur within a fraction of a microsecond at this level of beta-radiation exposure. At these fluxes, sputtering and knock-on damage can also be impactful.

When a nearly perfect crystal is the target, imaging through diffraction (capturing a diffraction tomography dataset) provides aberration-corrected resolution at fluxes which are low enough for even protein crystals to survive. Coincidentally, the same settings give the sharpest diffraction peaks, and the most numerous. This methodology has been applied to small molecules [3, 4] and proteins [5], and, to some extent, to materials science samples [6]. But its impacts and limits have not been widely explored in the materials science community. The technique can be used on insulators, crystals that are too thick for real space imaging, and those with complex structures (tens to millions of atoms in the basis) to obtain a 3-dimensional structure at a sub-angstrom resolution without an aberration corrector. When the molecular weight is too small for single particle analysis (about 50 kDa) [7], imaging through diffraction is one of the few options available.

We discuss the methods of achieving this resolution and some preliminary results using biological, small molecule, and materials science samples. Figure 1A shows an image of a typical MoO_3 crystal on a lacy carbon substrate. The crystal is ~100 nm thick and irregular. Real space imaging at atomic resolution (requiring less than 30 nm thickness) is not possible. Figure 1B shows the diffraction tomography data (also called 3D ED or microED) from the continuously rotated diffraction acquisition series using a flux of 0.01 $e^-/Å^2/s$. A 60° diffraction tomography dataset, corresponding to 80% crystallographic completeness, was collected using a total fluence of 3 $e^-/Å^2$. The highest resolution was determined to be 0.35 Å, which had 61.7% CC1/2 correlation at 0.1% significance level with a signal-to-noise ratio of 1.56. The lack of ±90° tilt appears as a missing wedge in reciprocal space, just as would appear in real space tomography. The image from the diffraction pattern (Figure 1C) shows a 3-dimensional reconstruction of the basis in our MoO_3 crystal at a resolution of 0.35 Å. The microscope was equipped with a 11 mm gap pole piece and an uncorrected 2.7 mm C_s and similarly sized C_c.

This resolution of 35 pm in the final reconstruction is achievable with modest investments in microscope optics and cameras. The methodology of this type of imaging will be discussed, along with a comparison between what could be imaged with a fluence of 3 $e^-/Å^2$ in real space and its limitations via the Rose Criterion, and further compared with other techniques [8].

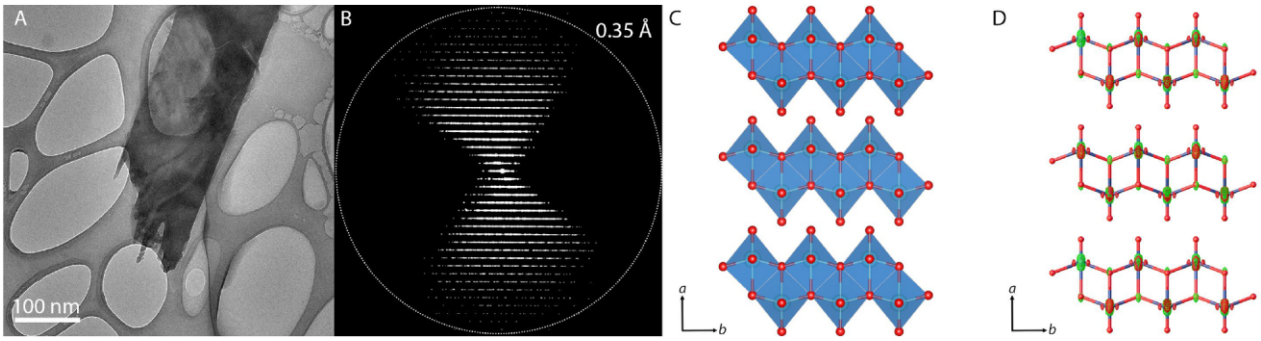

Figure 1. A) A TEM image of a typical MoO_3 crystal on a lacey carbon substrate. B) 3D reciprocal lattice from a continuously rotated diffraction acquisition series. C) The structure of MoO_3 determined from the 3D ED data. D) Difference potential map shown at 3σ level, calculated using spherical atomic scattering factors. The positive (green) and negative (red) peaks around each atom demonstrate the anisotropic features that become observable at 0.35 Å resolution.

References

1. T Yeates, *Lectures on Physical Biochemistry*.
2. I Usón and G M Sheldrick, *Curr. Opin. Struct. Biol.* **9**, (1999), **p.** 643-648.
3. C G Jones *et al.*, *ACS Cent. Sci.* **4**, (2018), **p.** 1587-1592.
4. D Zhang *et al. Zeitschrift fuer Kristallographie* **225**, (2010), **p.** 94-102.
5. Shi *et al.*, *eLife* (2013), **2:e01345**.
6. L Meshi and S Samuha, *Adv. Mater.* **30**, (2018), **1706704**.
7. R M Glaeser and R J Hall, *Biophys. J.* **100**, (2011), **p.** 2331-2337.
8. The authors acknowledge support from the Electron Imaging Center for Nanomachines (EICN) at the University of California, Los Angeles's California for NanoSystems Institute (CNSI) (RRID:SCR_022900). This work was supported by the BioPACIFIC Materials Innovation Platform of the National Science Foundation under Award No. DMR-1933487.